CEBAF: THE CONTINUOUS ELECTRON BEAM ACCELERATOR FACILITY AND ITS PHYSICS PROGRAM

Jean Mougey
Continuous Electron Beam Accelerator Facility
12000 Jefferson Avenue
Newport News, Virginia 23606 USA

Abstract

With the 4 GeV Continuous Electron Beam Accelerator Facility presently under construction in Newport News, Virginia, a new domain of nuclear and subnuclear phenomena can be investigated, mainly through coincidence experiments. An overview of the characteristic features of the accelerator and associated experimental equipment is given. Some examples of the physics programs are briefly described.

I. Introduction

During the last few decades, a wealth of information on the structure of nuclei has been obtained from electro-and photoinduced reactions. This follows from the intrinsic qualities of the electromagnetic probe: the basic interaction is given precisely by QED, leaving the hadronic current to be investigated as the only unknown. The smallness of the coupling allows the probe to explore the entire nuclear volume, and leads to the essential validity of the one photon exchange (Born) approximation (Fig. 1). Moreover, using electrons (i.e. "virtual" photons), additional kinematical flexibility is obtained by varying independently the energy transfer ν and the momentum transfer $\vec{q}$.

At energies below $\sim$ 1 GeV, models describing the nucleus as an assembly of essentially free nucleons moving in a mean effective potential have been quite successful. However, electrons and photons have given the clearest evidence for deviations from this "classical" picture, showing the role of mesonic currents, nucleon resonances and relativistic effects. Typical examples obtained from single arm electron scattering experiments are the deuteron electrodisintegration at threshold (Fig. 2), and the excitation energy spectrum in the continuum (Fig. 3) which cannot be explained quantitatively by simply adding the contributions from the quasielastic peak and the quasifree excitation of nucleon resonances.

At higher energies, one should expect to observe manifestations of the internal structure of hadrons, and the need to introduce the quark and gluon degrees of freedom explicitly. The challenging task for the future will be to search for such signatures, with the ultimate goal of understanding the nucleon-nucleon force at all distances in terms of quarks and gluons, and the role of the nucleon substructure in nuclear dynamics.

Although high energy inclusive reactions have given indications of QCD effects in the scaling (perturbative) region, no conclusive evidence has been obtained in the confinement (non-perturbative) one. One could expect clearer signatures from experiments in which reaction fragments are detected in coincidence with the electron. By observing specific

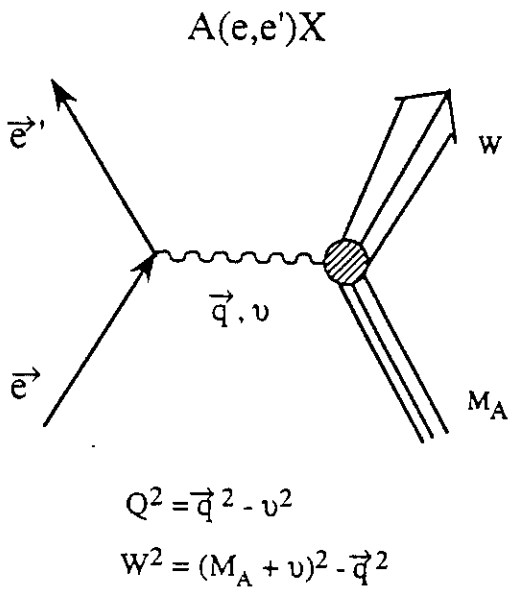

Figure 1. Inclusive electron scattering process in the "one photon exchange" (Born) approximation.

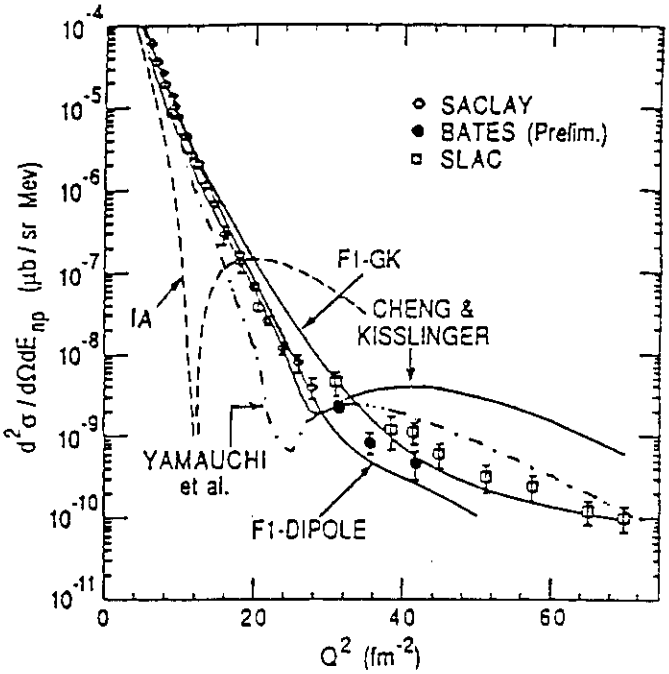

Figure 2. Selected data for the D(e,e')np reaction near threshold. Dashed curve: Impulse Approximation (nucleons only). Curves from Yamauchi *et al.* and Kisslinger *et al.* are results of Hybrid Quark Hadron models. Other curves are from nonrelativistic nucleons + mesons calculations (from ref. [1]).

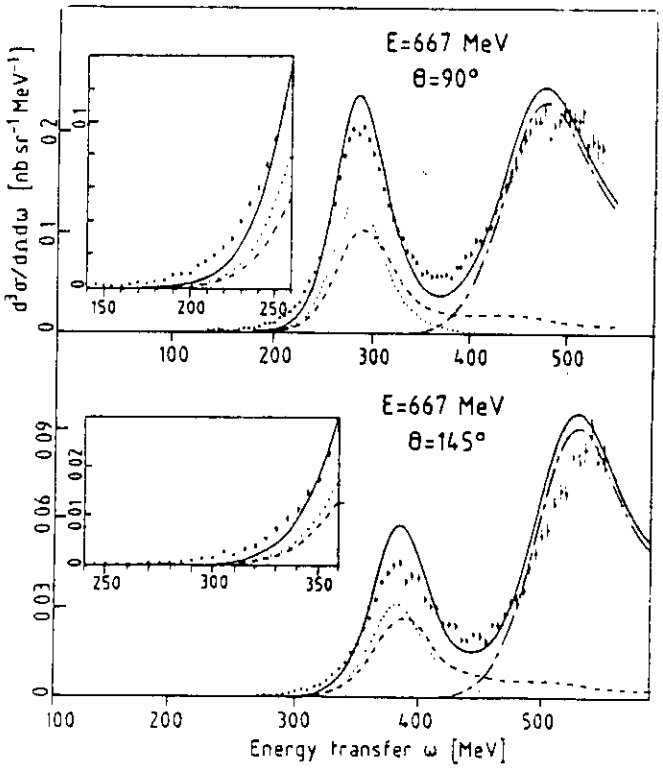

Figure 3. Cross sections for inclusive electron scattering off ^{3}He (from ref. [2]).

channels (one or two nucleon knock-out, pion or kaon production,$\cdots$) one should discriminate better between various aspects of the nuclear dynamics. However, these experiments are made difficult by the low duty cycle of existing electron accelerators, which restricts the kinematical domain in which acceptable true-to-accidental coincidence ratios can be obtained.

The new generation of electron accelerators in the multi-GeV range with nearly 100% duty cycle which are presently under construction or in project (see Table 1), will increase considerably the possibilities for such experiments.

Table 1

Facility	E_{max} (GeV)	duty cycle (%)	Completion date	Configuration
NIKHEF AmPS	0.83	90	1992	Linac + stretcher ring
Mainz MAMI-B	0.84	100	1991	3 stage microtron
MIT Stretcher	1	85	1992	Linac + stretcher ring
Bonn ELSA	3.5	30	1988	Synchroton + s.r., 200 nA
CEBAF	4	100	1994	5 pass SC recyclotron

In parallel, specific experimental techniques are currently being given strong R&D efforts, to allow full exploitation of the new accelerator capabilities. One can cite the following main examples:

a) High resolution magnetic spectrometers: Continuous wave acceleration produces beams of very high energy definition ($\sim 10^{-4}$) and very low emittance. Matching these characteristics, high resolution spectrometers allow not only the separation of discrete nuclear final states, but also a very precise determination of the kinematics, which has been shown to be needed for accurate absolute cross-section measurements. Designed with rather large angular ($\Delta\Omega \sim 10$ msr), momentum ($\Delta p/p \sim 10\%$) and luminosity ($L \sim 10^{38} cm^{-2} sec^{-1}$ or higher) acceptances, they allow precise measurements even for processes having very low cross-sections.

b) Large acceptance ($\sim 4\pi$) detectors: They are needed to perform exclusive high multiplicity experiments, or when the luminosity is intrinsically limited (real photon beams, polarized targets$\cdots$).

c) Polarized beams, targets, recoil polarimeters: As we will see later, more detailed information is obtained by separating the various nuclear responses associated with different polarization states of the virtual photon. New response functions can be reached when the beam, the target, and/or the detected ejectile is polarized. Especially interesting are responses in which the amplitude of interest, which could be small, interfere with the dominant one. A large number of these interference response functions can only be isolated by measuring the ejectile out of the scattering plane.

After a short description of the CEBAF accelerator and its experimental facilities, I shall discuss briefly some illustrative examples of the proposed experiments. Up to now,

65 physics proposals have been submitted to the CEBAF Program Advisory Committee, out of which 34 have been given initial beam time allocation, for a total of 437 beam days.

II. CEBAF accelerator and experimental equipment overview

CEBAF is a dedicated facility for nuclear physics in the several GeV range, the construction of which began in February 1987, in Newport News, Virginia[3]. The main beam performance objectives are:

Energy	0.5 to 4 GeV
Current intensity	0.1 to 200 μA
Duty cycle	100%, cw
Emittance (95%)	2 x 10^{-9} m rad
Energy spread (4σ(E)/E)	10^{-4}

The accelerating structure is based on a 5-cell, 1497 MHz superconducting cavity developed at Cornell and designed to provide at least 5 MV/m with $Q_o \geq 2.4 \times 10^9$ at 2K. Each cavity is individually powered by a 5 kW klystron. The accelerator configuration shown in Fig. 4 consists of two separate 0.4 GeV linac segments, connected by 180° achromatic and isochronous beam lines having large radii of curvature (5.1 m to 30.6 m) to minimize synchrotron radiation effects. A five pass recirculation scheme has been adopted for cost optimization.

The 45 MeV injector provides three interspersed 499 MHz trains [(1,4,7$\cdots$), (2,5,8,$\cdots$), (3,6,9$\cdots$)] of <2 ps bunches having individually adjustable current levels. Extraction at fractional energies, i.e. on the 1st to 4th pass, is accomplished by deflecting bunches with rf separators followed by septum magnets for simultaneous delivery to all three end stations of beams having different intensities (by a factor up to 1000) and different (correlated) energies. A polarized GaAs photocathode electron source has been developed in collaboration with University of Illinois[4]. The source can deliver up to 100 μA beams with 49% polarization. Various techniques are under investigation to increase the polarization rate.

Complementary sets of instruments[5] have been designed for the three experimental halls and are now under construction.

a) Hall A will have two identical, high resolution 4 GeV spectrometers (Fig. 5). Their characteristics are given in Table 2. The QQDQ design includes a large iron-dominated dipole with superconducting racetrack coils and focussing properties provided by slanted pole ends and a non-uniform field. The three superconducting quadrupoles are cos2θ-type, current-dominated magnets with higher multipole correcting coils. The detector systems include vertical drift chambers as position detectors ($\sim$ 100 μm track resolution) and a focal plane polarimeter in the hadron arm.

b) The CEBAF Large Acceptance Spectrometer (CLAS) to be installed in Hall B, together with a photon tagging facility, is a 6-coil superconducting toroidal magnet (Fig. 6) installed around the beam. The six sectors will be filled with drift chambers and particle identification detectors. The CLAS will be best suited for experiments for which broad kinematical coverage and high particle multiplicities are more important than resolution and high luminosity.

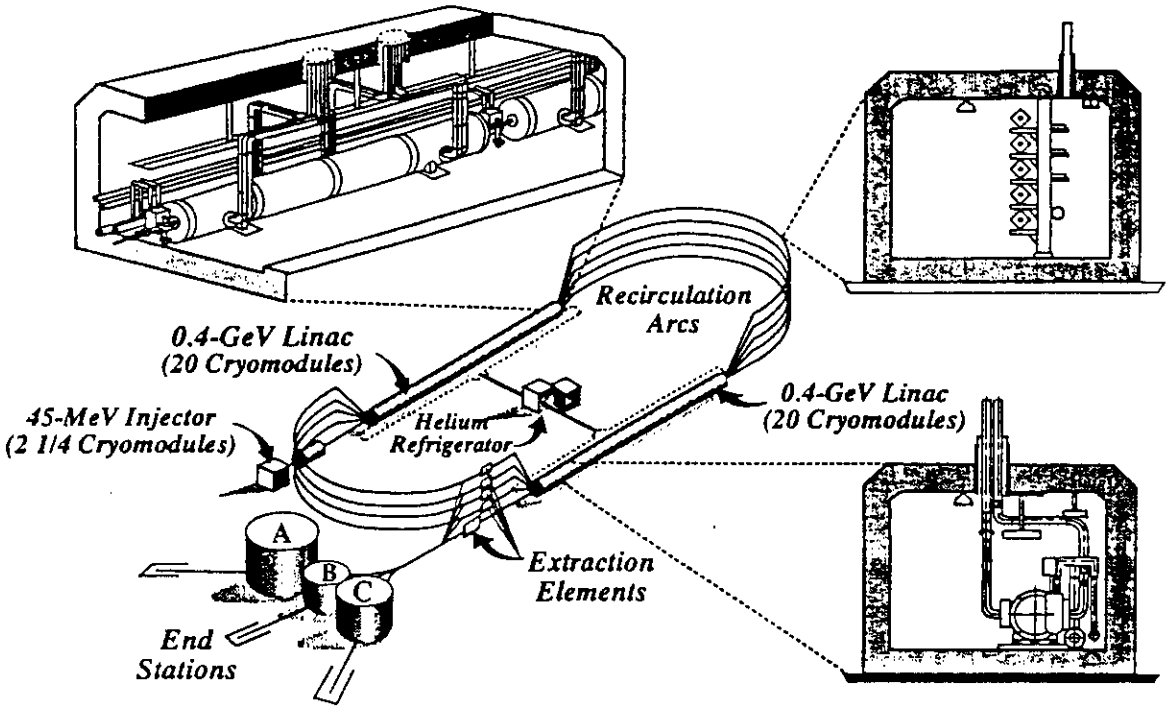

Figure 4. CEBAF accelerator configuration.

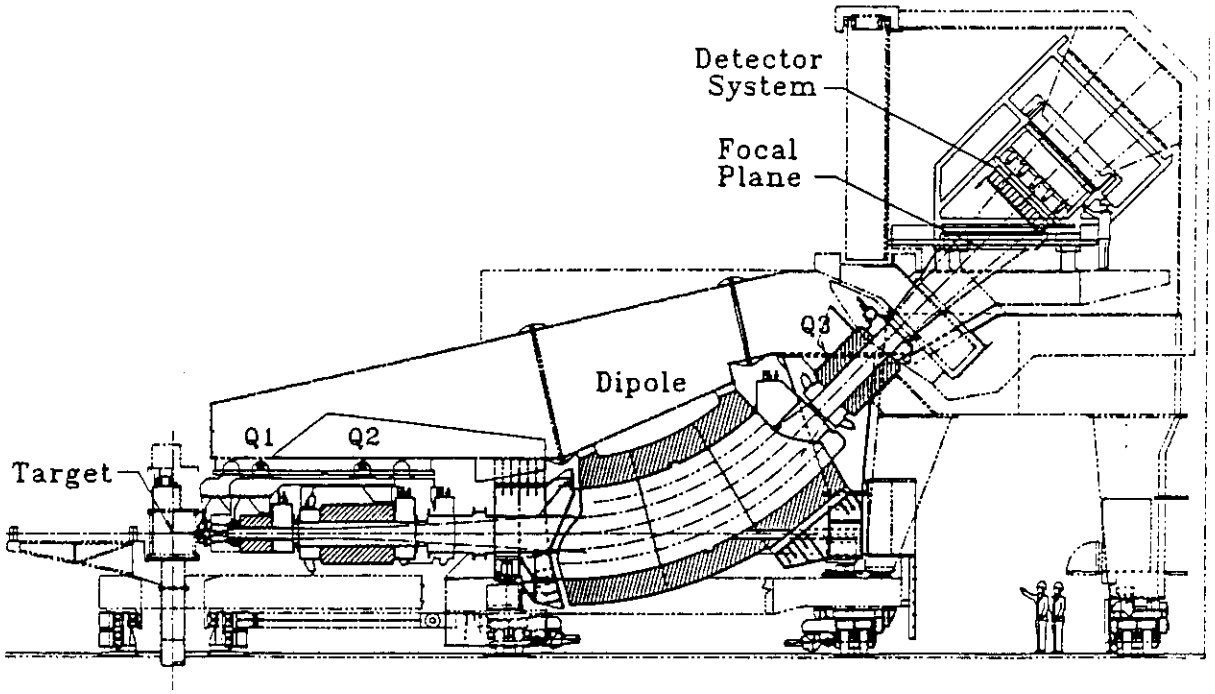

Figure 5. Hall A 4 GeV/c High Resolution Spectrometer

c) Hall C initial equipment (Fig. 7) will consist in a High Momentum 6 GeV/c Spectrometer (HMS) and a Short Orbit Spectrometer (SOS) (see Table 2). The moderate resolution ($\sim 10^{-3}$) should be sufficient for a substantial fraction of the few body physics program. The high momentum capability of the HMS will allow high-Q^2 physics. The SOS will be used for pion and kaon electroproduction experiments and for a variety of (e,e'p)experiments.

Table 2
CEBAF Spectrometer Characteristics

	Hall A HRS (2)	Hall C HMS	Hall C SOS
Configuration	QQDQ	QQQD	QD$\bar{\text{D}}$
Optical length (m)	23.4	24.8	7.4
Momentum range (GeV/c)	$0.3 \rightarrow 4$	$0.5 \rightarrow 6$	$0.2 \rightarrow 1.5$
Momentum acceptance (%)	10	10	40
Momentum resolution (FWHM)	10^{-4}	5×10^{-4}	2×10^{-3}
Angular range	$12.5^\circ \rightarrow 165^\circ$	$12.5^\circ \rightarrow 90^\circ$	$11.6^\circ \rightarrow 168^\circ$
Positioning accuracy (mr)	0.1		
Angular resolution: horiz. (mr)	0.5	0.4 (0.8)	
(FWHM) vert. (mr)	1.0	0.9 (0.8)	
Solid angle (msr)	7	6	9
Transverse length acceptance (cm)	10	10	10
Transverse position resolution (cm)	0.1	3.4 (0.6)	

Liquid and high density gas cryogenic targets are being developed in all three halls. The 1 kW cryotarget designed for Hall A will operate either with liquid H_2 and D_2 at 20K, 5 atm or with ^{3}He and ^{4}He gases at 20K (ultimately 10K) and 70 atm. With 15 cm cell length and 200 μA beam current, it corresponds to a luminosity of 5 x 10^{38}cm^{-2}s^{-1}. A polarized solid state NH_3 and ND_3 target is also being developed to operate initially (but not exclusively) in Hall C. Based on recent developments at MSU[6] one expects to reach nearly 100% polarization at 1K in a 5T magnetic field. Additional instrumentation will be provided by user groups. It may include neutron detectors and polarimeters[7], large solid angle scintillator arrays[8], a possible third arm 1.3 GeV/c Multipurpose Spectrometer (MPS)[9] and dedicated facilities for (e,e'K$^+$) and parity violation experiments.

The accelerator is scheduled to be completed by March 1993, with experiments starting in Hall C by June 1994. The HRS pair in Hall A and the CLAS detector in Hall B should be ready to take data by June 1995.

III. The structure of free nucleons

The precise knowledge of the electric and magnetic free nucleon form factors $G_E(Q^2)$ and $G_M(Q^2)$ up to the highest possible Q^2 value is of fundamental importance: first, as a testing ground for microscopic models of the internal structure of hadrons and the γ_vNN coupling, second as a basic ingredient in the analysis of electron-nucleus data. Ultimately,

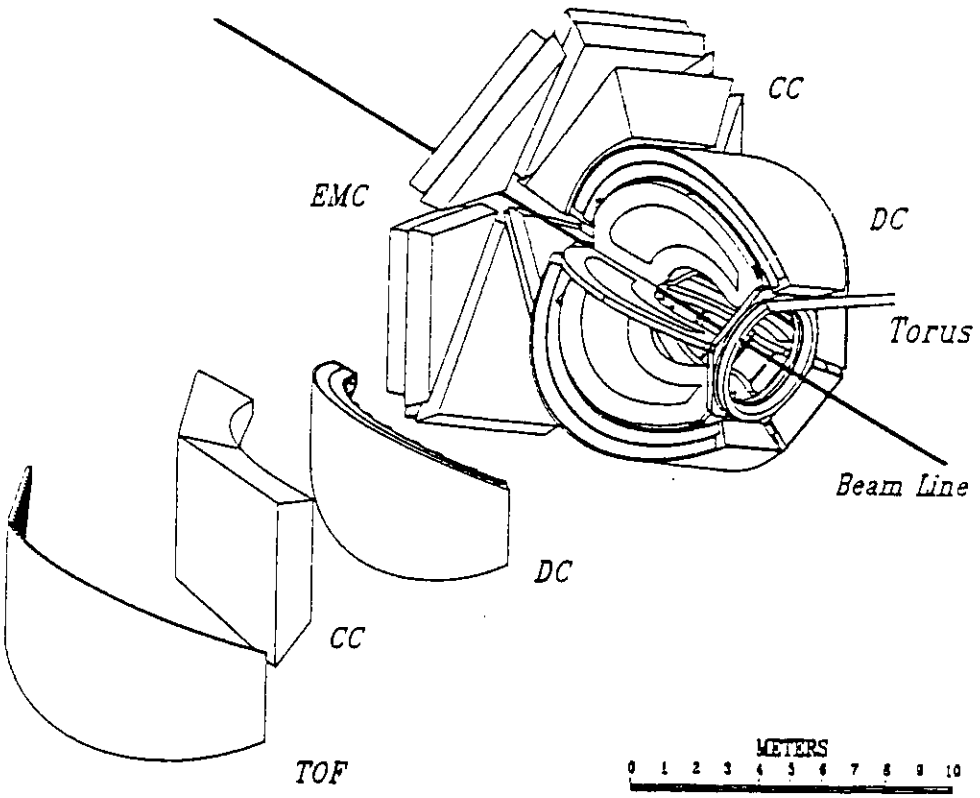

Figure 6. The CEBAF Large Acceptance Spectrometer (CLAS). Drift chambers (DC), time-of-flight counters (TOF), gas Cerenkov counters (CC) and electromagnetic calorimeters (EMC) provide particle tracking and identification. Main characteristics include: θ-range: 8° - 140°; ϕ-range (% of 2π) = 85 (50) at $\theta = 90°(10°)$; momentum resolution $\leq 1\%$ (FWHM); maximum luminosity $\simeq 10^{34}$ cm^{-2}s^{-1}; π/K (π/p) separation up to 2(3) GeV/c.

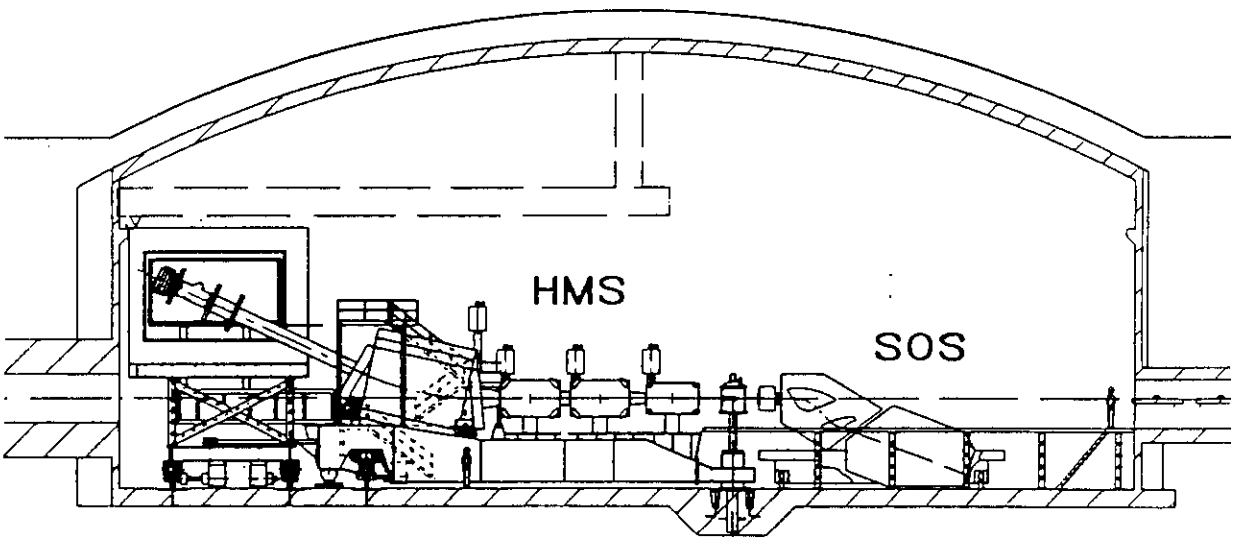

Figure 7. Hall C High Momentum Spectrometer and Short Orbit Spectrometer.

understanding these form factors is the first step towards understanding the structure of nucleons and nucleon resonances inside nuclei, and the quark hadronization mechanisms.

III.1 Proton electric form factor

Although precise elastic ep cross section data exist up to $Q^2 \approx 31$ $(GeV/c)^2$ [10], G_{Ep} is rather poorly known above $Q^2 = 1(GeV/c)^2$, as shown in Fig. 8. The usual Rosenbluth separation technique to isolate G_{Ep} and G_{Mp} becomes more and more difficult at high Q^2 as the relative contribution of G_{Ep} becomes smaller. Yet, it has been used recently at SLAC to measure G_{Ep} up to $Q^2 = 7$. Preliminary results have been reported, with $\sim \pm$ 20% uncertainties[11]. A more promising technique for determining G_{Ep} is to measure the interference term that results when longitudinally polarized electrons are incident on either a polarization proton target or when the recoil proton polarization is detected[12]. The recoil polarization technique will be used by Perdrisat et al.[13] to obtain a few percent measurement of G_{Ep} up to Q^2=4.5 $(GeV/c)^2$. By measuring both the transverse and longitudinal components of the proton polarization vector, the quantity G_{Ep}/G_{Mp} can be obtained without precise determination of the beam polarization and polarimeter analyzing power.

III.2 Neutron electric form factor

The electric form factor G_{En} of the neutron is poorly known at all Q^2 except around Q^2=0. For Q^2 up to ~ 0.7 $(GeV/c)^2$ G_{En} has been extracted from elastic e-d scattering[14], but the values depend on the model chosen for the deuteron wave function. As in the case of G_{Ep}, G_{En}/G_{Mn} can be determined in a model independent way by measuring the polarization component of the recoil neutron perpendicular to $\vec{q}$, in the scattering plane, using the reaction $D(\vec{e},e'\vec{n})p$ at the quasielastic kinematics. Following a similar experiment at Bates, Madey et al. will determine G_{En} at CEBAF in the range $0.15 < Q^2 < 1.5$ $(GeV/c)^2$ with $\Delta G_{En} \sim \pm$ 0.015[15]. Another method to measure G_{En}/G_{Mn} is through a polarization asymmetry measurement in the reaction $\vec{D}(\vec{e},e'n)p$ on a vector polarization deuteron target. This technique will be used in Hall C by Day et al[16], with the polarization NH_3 and ND_3 targets under development at University of Virginia. Anticipated results of both methods are shown in Fig. 9 along with various theoretical predictions.

III.3 The nucleon weak form factors

In elastic $\vec{e}N$ scattering using longitudinally polarized electrons, parity violating contributions arise from the interference between the one-photon exchange (electromagnetic) amplitude and the neutral boson Z^o (weak) exchange one (Fig. 10). More explicitly, the parity violating asymmetry $A_{\vec{e}p} = \frac{\sigma_+ - \sigma_-}{\sigma_+ + \sigma_-} \sim \frac{A_{em}A_w}{|A_{em}|^2}$ writes

$$A_{\vec{e}p} = \frac{G_F Q^2}{\pi\alpha\sqrt{2}} \cdot \frac{\epsilon G_E^\gamma G_E^Z + \tau G_M^\gamma G_M^Z - \frac{1}{2}(1-4\sin^2\theta_w)\sqrt{1-\epsilon^2}\sqrt{\tau(1+\tau)}G_M^\gamma G_A^Z}{\epsilon(G_E^\gamma)^2 + \tau(G_M^\gamma)^2}$$

In the Standard Model, and invoking strong isospin symmetry the weak form factors are

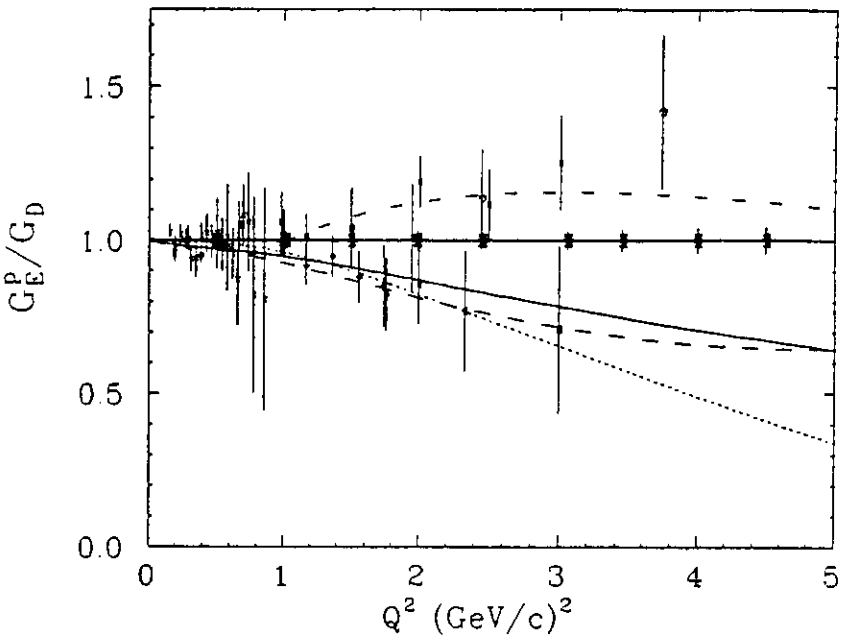

Figure 8. Data and theoretical models for the proton electric form factor G_{Ep}. Solid curve: Gari and Krümpelmann; long dashes: Höhler et al.; short dashes: Iachello et al.; dot-dashed: Radyushkin. The filled circles are the projected data points from CEBAF PR-89-014[13].

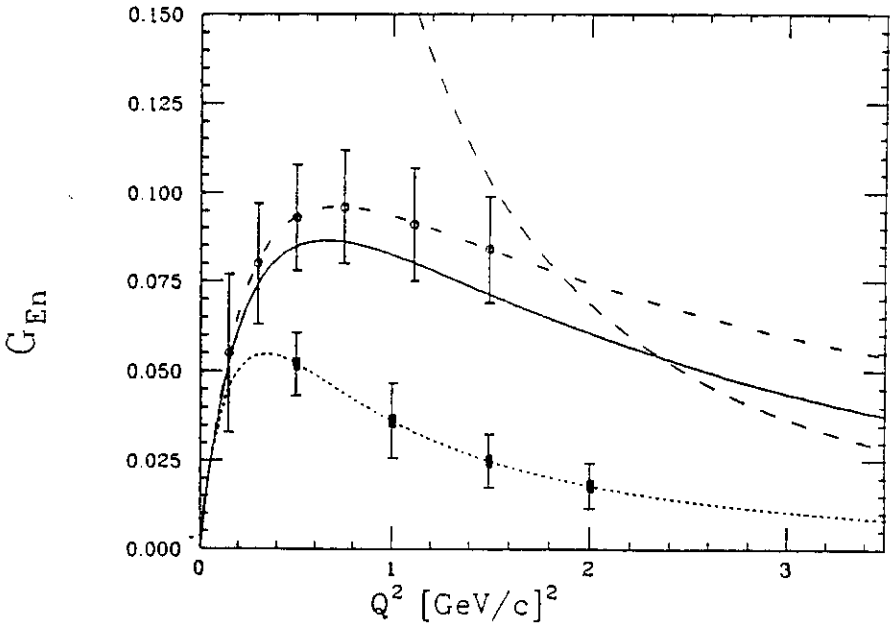

Figure 9. Theoretical predictions for the neutron electric form factor G_{En}. Solid curve: Gari and Krümpelmann; short dashes: Galster et al.; dot-dashed: G_{En}, dipole form; long-dahsed: G_{Ep}, dipole form. Open circles: expected data points, based on Galster calculation, for the CEBAF recoil polarization experiment[15]. Filled circles: expected data points, based on the dipole form, for the target polarization experiment[16].

related to the electromagnetic ones through

$$G_E^Z = (\frac{1}{4} - \sin^2\theta_w)G_{Ep}^\gamma - \frac{1}{4}G_{En}^\gamma - \frac{1}{4}G_E^s$$
$$G_M^Z = (\frac{1}{4} - \sin^2\theta_w)G_{Mp}^\gamma - \frac{1}{4}G_{Mn}^\gamma - \frac{1}{4}G_M^s$$

where $G_{E,M}^s$ come from the strange quark current $\bar{s}\gamma_\mu s$.

The term with G_A^Z is suppressed since (1-4 $\sin^2\theta_w$) is small. Therefore, one can separate G_E^Z and G_M^Z by varying the electron kinematics (i.e. ϵ) at given Q^2. An experiment is in preparation at MIT-Bates[17] to determine G_M^s at $Q^2 \sim 0.1$ (GeV/c)^2 by measuring $A_{\vec{e}p}$ at backward angles. By performing the measurement at forward angle, one can get information about G_E^s, therefore about the "strangeness radius" of the proton[18,19].

Such measurements have been proposed at CEBAF. In one case[20,21], the two Hall A spectrometers are used at the most forward angle (12°5) to measure the asymmetry in elastic $\vec{e}$p and $\vec{e}$ ^{4}He in the range $Q^2 = 0.2$ to 1.3 (GeV/c)^2. With typical running times of $\sim$ 300 hrs per data point, uncertainties $\Delta A/A$ of 10% to 30% are expected, according as high luminosity integration or low luminosity counting methods are used. In the other case[22], a dedicated instrument - an 8-coil toroidal spectrometer - could be used to measure the elastically scattered proton at $\theta_p \sim 65°$ - 80°, corresponding to $Q^2 = 0.1$ to 0.3 (GeV/c)^2.

IV. (e,e'N) reactions

IV.1 General features, Polarization experiments

The simplest interpretation of the (e,e'N) reaction in the quasielastic regime is that the electron scatters on a single proton which is ejected (Fig. 11). Assuming further no final state interactions (PWIA) the coincidence cross section takes the simple form

$$\frac{d\sigma}{d\vec{e}\,'d\vec{p}\,'} = K\sigma_{ep}S(\vec{p}_m, E_m)$$

where σ_{ep} is essentially the free elastic e-p cross section and $S(\vec{p}_m, E_m)$, the spectral function, i.e. the joint probability for removing a proton of momentum $\vec{p}_m$, leaving the residual system with an excitation energy $E_m - E_m^o$, E_m^o being the separation energy of the least bound proton. In an independent particle shell model

$$S(\vec{p}_m, E_m) = \Sigma_\alpha |\phi_\alpha(\vec{p}_m)|^2 \delta(E_m + E_\alpha)$$

where ϕ_α is the wave function of the single particle (hole) state $\alpha = \{n\ell j\}$ and E_α its binding energy. Although final state interactions (FSI) and meson exchange currents (MEC) introduce significant corrections to this picture, important information has been obtained on single nucleon densities up to $\sim$ 600 MeV/c for D, ^{3}He and ^{4}He and $\sim$ 300 MeV/c for heavier nuclei[23]. A beautiful example of what is currently achieved at NIKHEF is shown in Fig. 12 for the ^{208}Pb(e,e'p) reaction[24] where several states in the 0-4 MeV region are clearly identified ($\delta E_m \sim 120$ keV), with specific momentum distributions.

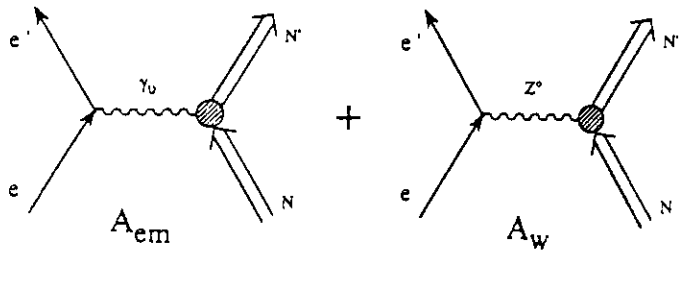

Figure 10. Electromagnetic (A_{em}) and weak (A_W) amplitudes in elastic eN scattering.

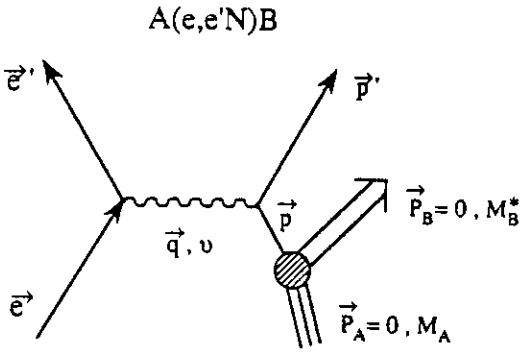

$$E_m = M_B^* + M_p - M_B$$

$$\vec{p}_m = -\vec{p}_B$$

Figure 11. Direct nucleon knock-out process in Plane Wave Impulse Approximation (PWIA).

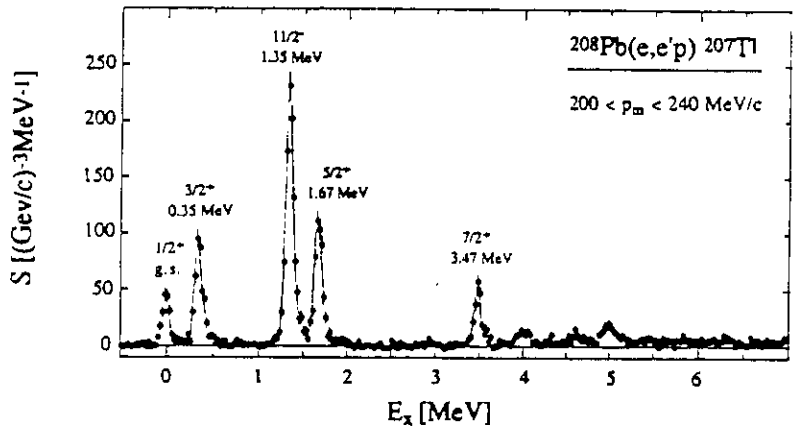

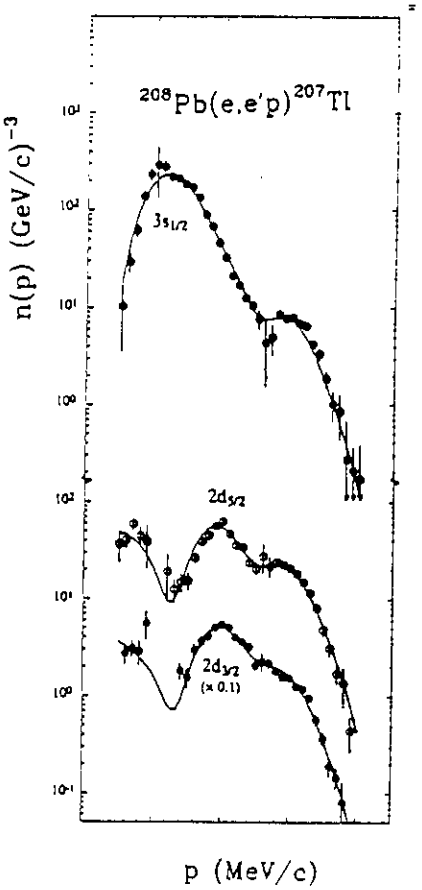

Figure 12. Left: Missing energy spectrum for ^{208}Pb(e,e'p) obtained at NIKHEF[24]. Right: Spectroscopic factor for different orbitals plotted as a function of distance from the Fermi surface.

However, limits of this simple picture have also been evidenced. Attempts to determine occupation probabilities for simple cases where the residual state can be modeled as a single-hole state in the target nucleus have yielded values smaller than expected[25]. Strength is missing in the "shell model" region. Distorted wave impulse approximation calculations have not been successful to describe consistently data taken over a range of kinematics. As for inclusive (e,e') scattering, ratios of longitudinal to transverse response have been difficult to explain[26,27,28]. Substantial contributions from other mechanisms - meson exchange currents, multinucleon emission, $\cdots$ - have been found in the same kinematical region[29]. Finally, a large amount of strength has been found at high missing energy[30] which also defies explanation within simple models.

Deeper insight into the various mechanisms leading to nucleon emission could be obtained from separate determination of the various response functions which appear in the most general form of the (e,e'X) coincidence cross section. As an example, with the kinematical notations of Fig. 13, the $(\vec{e},e'p)$ cross section for longitudinally polarized (helicity h) electrons is

$$\frac{d\sigma^h}{d\vec{e}\,'d\vec{p}\,'} = \sigma_o \cdot \frac{1}{2}[1 + hA]$$

where

$$\sigma_o = K\{v_L R_L + v_T R_T + v_{TT} R_{TT} \cos 2\alpha + v_{LT} R_{LT} \cos\alpha\}$$

is the unpolarized cross section and

$$A = \frac{K}{\sigma_o} \times v_{LT}, R'_{LT} \sin\alpha$$

is the electron analyzing power. K and the v_{ij} are kinematical factors (electron kinematics only). All information on the nuclear currents is contained in the 5 (Lorentz invariant) nuclear responses R_{ij}. A complete separation would necessitate out-of-plane measurements. Similarly, if the recoiling proton polarization is measured[31], one gets

$$\frac{d\sigma^{h,s'}}{d\vec{e}\,'d\vec{p}\,'} = \sigma_o \cdot \frac{1}{2}[1 + hA + (\vec{P} + h\vec{P}\,') \cdot \vec{\sigma})]$$

where $\vec{P}(P_n, P_\ell, P_t)$ is an induced polarization containing 8 new responses and $\vec{P}'(P'_n, P'_\ell, P'_t)$ the polarization transfer (5 new responses). Being spin-dependent quantities, these new response functions show specific and sometimes strong dependence on particular aspects of the reaction dynamics like off-shell and relativistic effects, exchange currents and many body dynamical effects. Further investigations of their specific sensitivities together with studies of experimental separation techniques are clearly needed. Particularly attractive are the parallel kinematics (only 5 out of 18 response functions survive) and cases where a given function can be isolated by simply reversing the incident beam polarization or measuring an asymmetry in the proton polarimeter.

Clearly, coincidence (e,e'N) experiments will constitute an important fraction of the CEBAF physics program. Some examples are given here, taken among the approved experiments.

IV.2 Coincidence D(e,e'p)n experiments

High precision systematic studies of the D(e,e'p)n reaction will be performed with the Hall A spectrometers. The Q^2-dependence of the reaction will be examined by performing longitudinal/transverse separations for protons emitted along $\vec{q}$ at $0.25 < Q^2 < 3.5$ (GeV/c^2) and p_n=0. The proton angular distribution will be measured up to p_n=500 MeV/c at $|\vec{q}| = 1$ GeV/c. From in-plane measurements on either side of $\vec{q}$, plus a backward angle measurement, R_T, R_{LT} and $R_L + R_{TT}$ can be separated and will provide stringent tests of the microscopic models of the reaction[32].

Additional tests of the deuteron structure and reaction mechanism will be provided by measurements of all six polarization observables which can be obtained from coplanar $D(\vec{e}, e'\vec{p})$ experiments[33]. Detailed non-relativistic calculations have been performed at 900 MeV incident energy by Arenhövel et al.[34] showing the sensitivity of the polarization components (corresponding to the $R^t_{LT'}, R^\ell_{TT'}$ and $R^n_{LT'}$ response functions respectively) to meson-exchange currents (MEC), isobar configurations (IC) and final state interactions (FSI). Similar conclusions have been reached by Shebeko et al[35]. At higher energies, relativistic calculations have been performed by Rekalo et al.[36] and are underway by Gross and Van Orden[37]. The measurements will be performed at fixed $|\vec{q}| = 1.26$ GeV/c going up to $p_n = 300$ MeV/c both sides of $\vec{q}$. By varying Q^2 at p_n=0 the outgoing proton energy will vary from 0.13 to 1.7 GeV, providing a rigorous test of the description of the two-nucleon scattering state.

IV.3 High momentum components and short-range correlations

Recent (e,e'p) experiments on ^{3}He and ^{4}He have demonstrated clearly the link between high momentum components and short distance nucleon-nucleon interactions[29,38]. Recoil momentum distributions have been obtained up to $p_m \sim 0.6$ GeV/c for the two- and many-body break up channels. Results for ^{4}He (Fig. 14) show that momenta larger than $\sim$ 350 MeV/c reside mostly in the many-body break up channels. The missing energy spectra show a broad structure in the continuum which moves towards higher E_m as p_m increases, in quantitative agreement with what would be expected from the disintegration of a nucleon pair at rest. The width reflects the center-of-mass motion of the pair. At CEBAF, it is proposed to vastly extend the range of these studies, first by precise measurements on ^{3}He, ^{4}He[39] and ^{16}O [40], allowing the separation of three unpolarized response functions at Q^2 up to 1 (GeV/c)^2, for recoil momenta up to 1 GeV/c. A better characterization of the contributing processes will be possible, since some of them, like MEC, affect primarily the transverse responses.

The next step is obviously to detect the partner nucleon in the pair in a triple coincidence (e,e'2N) experiment. The CEBAF beam characteristics will allow the development of such experiments, very difficult to perform at lower energy (< 1 GeV) and duty factor ($\leq$ 1%) accelerators. Broad surveys of multi-nucleon emission processes using the CLAS have been proposed[41] with measurements of total yields, angular and energy distributions for (e,e'N), (e,e'2N), (e,e'Nπ), (e,e'2Nπ)$\cdots$ reactions. This will allow the decomposition of the inclusive or semi-exclusive cross-section into well-identified multiparticle final states, and to obtain a first shot at more specific aspects like three-body currents, nucleon-nucleon

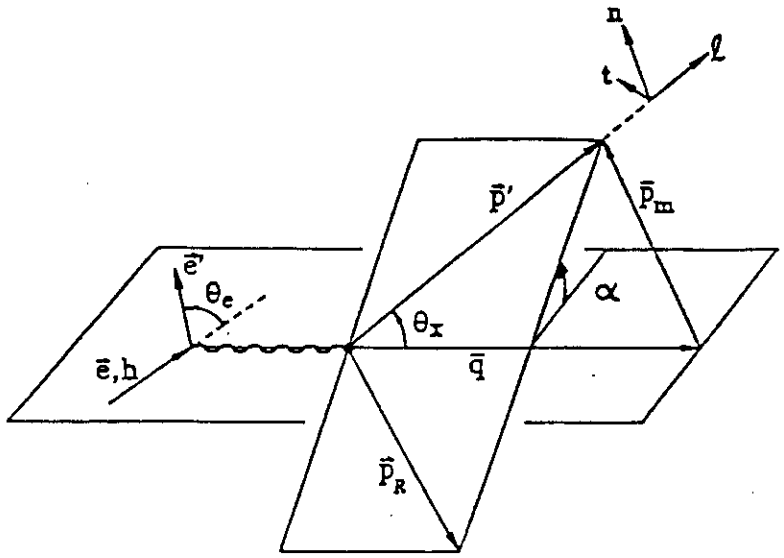

Figure 13. Kinematical notations for the A($\vec{e}$,e'$\vec{p}$)X reaction.

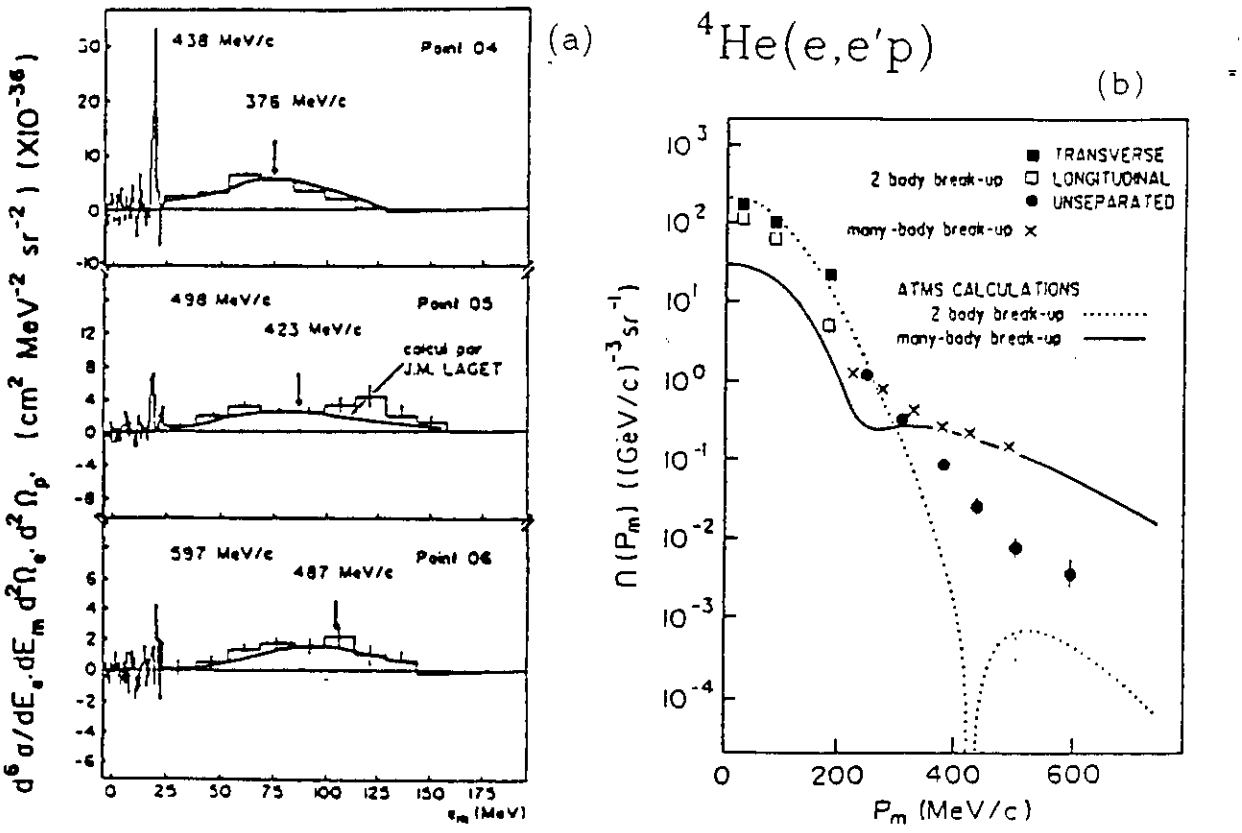

Figure 14. Experimental missing energy spectra (a) and proton momentum distributions (b) from the ^{4}He(e,e'p) reaction[38]. At high recoil momenta, the strength is dominantly at high missing energies in the many-body channels.

ground state correlations and possible signatures of multiquark clusters (6q, 9q$\cdots$). More detailed studies have been proposed using Hall A spectrometers. The ^{4}He(e,e'd) reaction cross section will be measured in the range $0.23 < Q^2 < 1.95$ (GeV/c)^2 for both d-d and d-pn break-up channels[42]. Triple arm (e,e'pn) and (e,e'2p) experiments on ^{3}He and ^{4}He have also been proposed in Hall A using existing neutron (University of Virginia) or proton (NIKHEF) scintillator arrays as second hadron detection arms[43], or possibly using the MPS[9]. Various kinematics with momentum transfers up to Q^2=1 (GeV/c)^2 and relative momenta in the initial pair NN up to 900 MeV/c have been considered. Although the (e,e'pn) reaction cross section is larger by nearly two orders of magnitude, the (e,e'2p) reaction looks more promising. One expects two-body processes to be strongly suppressed in the transverse part, which then can be used to study three-body forces[44].

IV.4 Q^2 dependence: bound nucleon structure, hadronization

By measuring the Q^2 dependence of the (e,e'N) reaction cross-section, information can be obtained about possible modifications of nucleon electromagnetic properties in the nuclear medium, and about the role of the quark-gluon degrees of freedom in nucleon emission processes.

Renewed interest was given to the issue of the nucleon structure in the nuclear medium by the observation of the EMC effect and of the "missing" longitudinal strength in the nuclear response at moderate Q^2 values. Indeed, from the data presently available, ^{4}He is the lightest nucleus for which a significant suppression of the longitudinal strength ($\tilde{\sim}$ 20% after all corrections) is observed in quasielastic (e,e'p) scattering (see Fig. 15)[45]. However, the Q^2-dependence in the measured range of 0.1 - 0.4 (GeV/c)^2 appears to be consistent wit the one expected from a free nucleon. This result is consistent with inclusive (e,e') data from Bates[46] at Q^2 values up to 0.4 (GeV/c)^2, but differ from recent (e,e') results obtained at SLAC (experiment NE9[47]) at Q^2=0.88 (GeV/c)^2, which are consistent with no longitudinal suppression. At CEBAF, precise measurements will be performed[39] on both ^{3}He and ^{4}He, over a wide Q^2 range of 0.3 - 4 (GeV/c)^2 at p_m=0 with additional measurements at Q^2=0.5 and 1 (GeV/c)^2 at p_m=$\pm$300 MeV/c.

At higher Q^2, the full momentum transfer is carried out initially by a single quark which "hadronizes" in the nuclear medium. At the quasielastic peak, the "proton" is formed as a small size ($\sim \frac{1}{Q}$) color neutral object, which expands on its way out of the nucleus. Its interaction with the medium being weaker than that of a normal size nucleon, this gives rise to the "color transparency" phenomenon. Several experiments[48,49] have been designed to investigate the possible onset of this effect in the CEBAF energy range. As shown in Fig. 16, one of the most sensitive observables is the induced polarization component P_n which vanishes in the absence of final state interaction. This component will be measured for the $(e,e'\vec{p})$ reaction on ^{2}He, ^{4}He and ^{16}O, in the Q^2 range of 1 to 6 (GeV/c)^2 [49].

V. Electromagnetic excitation of baryon resonances

Systematic studies of the electromagnetic transition from the free nucleon to resonances below $\sim$ 2 GeV are expected to yield fundamental information on the γ_vNN* vertex as well as on the baryon substructure and the quark and gluon dynamics in confined

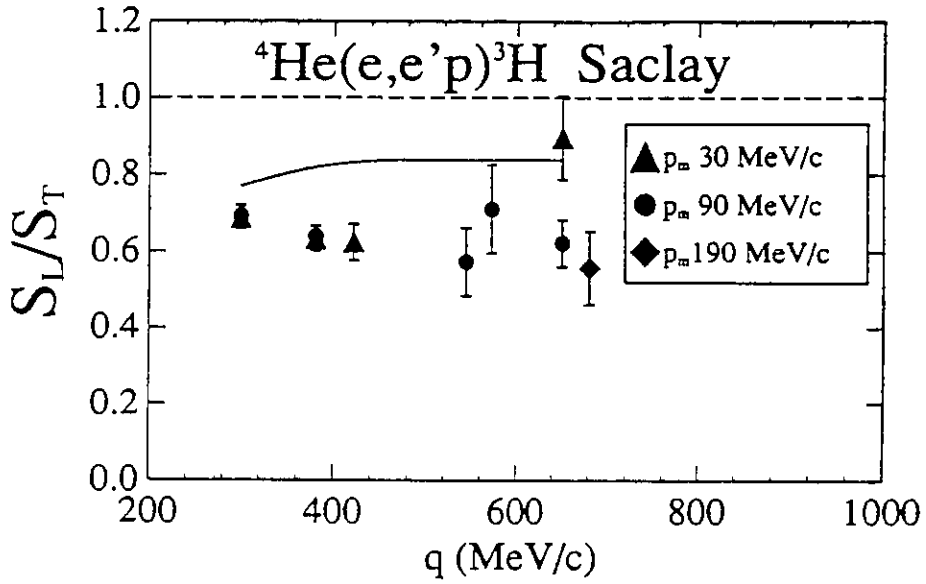

Figure 15. Ratio of longitudinal to transverse spectral functions for the reaction ^{4}He(e,e'p)^{3}H. The experimental data are compared to PWIA (dashed line) and a calculation by J.M. Laget including final state interactions and meson exchange currents (from ref. [45]).

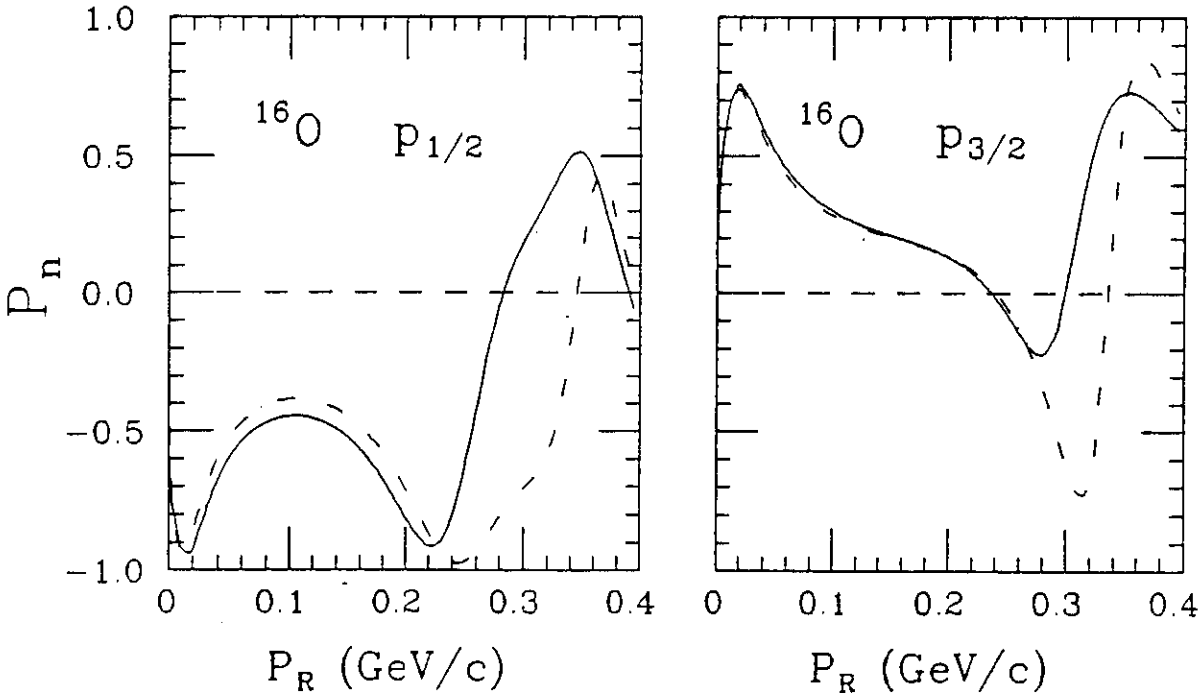

Figure 16. The induced polarization vector P_n in the ^{16}O(e,e'$\vec{p}$) reaction leading to $1p_{1/2}$ (left) and $1p_{3/2}$ (right) hole states, for E_o=4 GeV and Q^2=0.93 (GeV/c)^2. Curves are from Dirac DWIA (solid) and nonrelativistic DWIA (dot-dashed) calculations from ref. [31]. Note that P_n vanishes in PWIA (dashed line).

systems. The γ_vNN* vertex (Fig. 17) is described by three amplitudes $A_{\frac{1}{2}}(Q^2)$, $A_{\frac{3}{2}}(Q^2)$ and $S_{\frac{1}{2}}(Q^2)$, where A and S correspond to transverse and longitudinal (scalar) coupling, respectively, and the subscripts refer to the total helicity of the γ_vN system. Coincident detection of the resonance decay products, which will be possible in the CLAS detector, allow the separation of overlapping resonances and spin/isospin assignments. Moreover, polarization measurements give information on the imaginary part of the amplitudes, therefore on the relative phases.

Information should be obtained about the nature of the transition (single or multiquark), the wave function of the excited state and the confinement potential. One would like also to search for "missing" states predicted by QCD motivated extensions of the non-relativistic quark model[50], which tend not to couple to the πN channel. At high Q^2, one may observe the transition from non-perturbative to perturbative regime.

Electro- and photo-excitation of nucleon resonances will be a major program at CEBAF, mostly for the Hall B CLAS detector[51]. A few examples have been selected here.

V.1 The transition $\gamma_v N \rightarrow \Delta\ (1232) \rightarrow N\pi$

In SU(6) symmetric quark models, this transition is explained by a single quark spin-flip in the L=0 3-quark ground state, corresponding to a magnetic transition M_{1+}. In more elaborate QCD based models including color hyperfine interactions (color magnetism), the Δ acquires L=2 components, leading to small electric E_{1+} and scalar S_{1+} contributions (Fig. 18). At very high Q^2, PQCD predicts $E_{1+}/M_{1+} \rightarrow 1$, while S_{1+}/M_{1+} remains small. Unpolarized measurements of the reactions $p(e,e'p)\pi^o$ and $p(e,e'\pi^+)n$ in the CLAS[52] will provide information about $|M_{1+}|^2$, $Re(E_{1+}M^*_{1+})$ and $Re(S_{1+}M^*_{1+})$. Electron asymmetry will give $I_m(S_{1+}M^*_{1+})$[53]. A polarization transfer $p(\vec{e},e'\vec{p})\pi^o$ experiment has been also proposed in Hall A at $Q^2 = 0.5$, 1 and 1.5 $(GeV/c)^2$ [54]. Information about $Im(E_{1+}M^*_{1+})$ will be obtained, as well as precise determination of individual response functions which provide more stringent constraints on models.

V.2 The transition $\gamma_v N \rightarrow P_{11}\ (1440) \rightarrow N\pi$

The P_{11} (1440) Roper resonance is treated in the simplest quark model as a single quark radial excitation $(1s)^3 \rightarrow (1s)^2\ (2s)^1$. Therefore, the transition should have a large Coulomb monopole (longitudinal) component, along with the magnetic dipole one. However, the existence of the Roper in electroproduction data remains uncertain. Recent theoretical works[55] have indicated a possible description of the Roper as an hybrid $|3q,g>$ state, which would mean a purely magnetic transition. Relativistic quark model calculations[56] produce almost no longitudinal contribution. Several experiments in the CLAS, as well as a polarization transfer experiment $p(\vec{e},e'\vec{p})\pi^o$ in Hall A[54] will study the Q^2 dependence of the N $\rightarrow$ Roper transition. Fig. 19 shows the sensitivity to models of some of the response functions which will be separated in the Hall A experiment.

V.3 Baryon resonance studies a high Q^2

Measurements of the Q^2 dependence of the N $\rightarrow \Delta$, N* transition form factors up to the highest Q^2 values provide essential information about the internal wave function of the

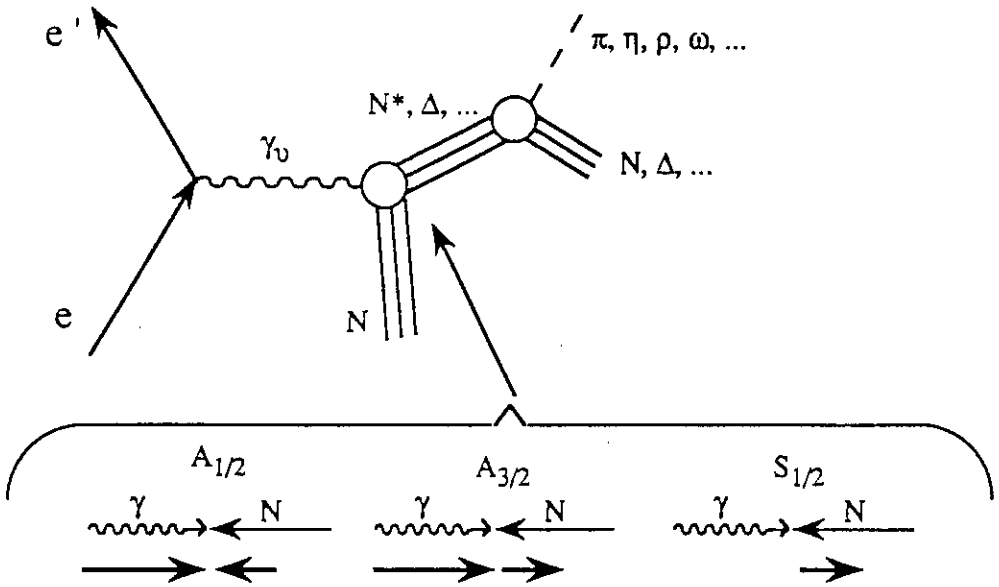

Figure 17. Diagram for electroexcitation of baryonic resonances on the free nucleon and their subsequent decay. The $\gamma_v NN^*$ vertex is described by three helicity amplitudes.

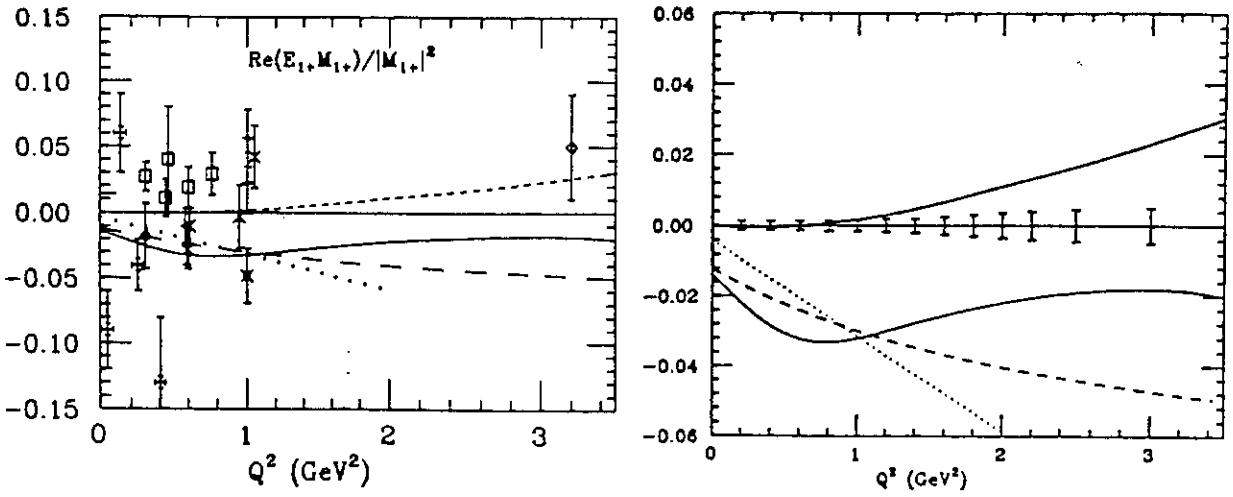

Figure 18. Interference term $Re(E_{1+}M_{1+}^*)/|M_{1+}|^2$ for the $\gamma_v p \rightarrow \Delta^+(1232)$ transition: a) existing data compared with model calculations (from ref. 51); b) expected statistical errors from CEBAF PR-89-037[52].

resonances. Indeed, separated data on the helicity asymmetry $\mathcal{A}=(A_{\frac{1}{2}}^2 - A_{\frac{3}{2}}^2)/(A_{\frac{1}{2}}^2 + A_{\frac{3}{2}}^2)$ for the transition to $D_{13}(1520)$ and $F_{15}(1688)$ resonances show a rapid evolution from $A_{\frac{3}{2}}$ dominance at low Q^2 to $A_{\frac{1}{2}}$ dominance above 0.6-0.7 $(GeV/c)^2$. Perturbative QCD predicts the following asymptotic behaviour

$$A_{\frac{1}{2}}(Q^2) \rightarrow C_1/Q^3 \qquad A_{\frac{3}{2}}(Q^2) \rightarrow C_2/Q^5 \qquad Q^2 \rightarrow \infty$$

For the Δ, $A_{\frac{1}{2}}$ dominance would imply $M_{1+} = E_{1+}$, whereas experimentally one finds $E_{1+} << M_{1+}$ in the region where the crossover appears to occur for the D_{13} and F_{15}. More high quality measurements at CEBAF up to $Q^2 \sim 4$ $(GeV/c)^2$ in the region W=1.2 to 1.8 GeV[57] should improve considerably the experimental situation on this subject.

V.4 Photo- and electroproduction of hyperons

Existing data on the elementary process $\gamma p \rightarrow K^+Y$ ($Y = \Lambda, \Lambda^*, \Sigma, \Sigma^*$) are scarce and of rather poor quality. More detailed and precise experiments will bring information on the production mechanisms and the KYN, KYN* coupling constants, essential for future electromagnetic studies of hypernuclei. Using the CLAS detector, one can observe the hyperon decay and, in the case of the Λ, obtain its polarization[58]. Polarization transfer measurements using polarized electrons to produce circularly polarized photons are also planned.

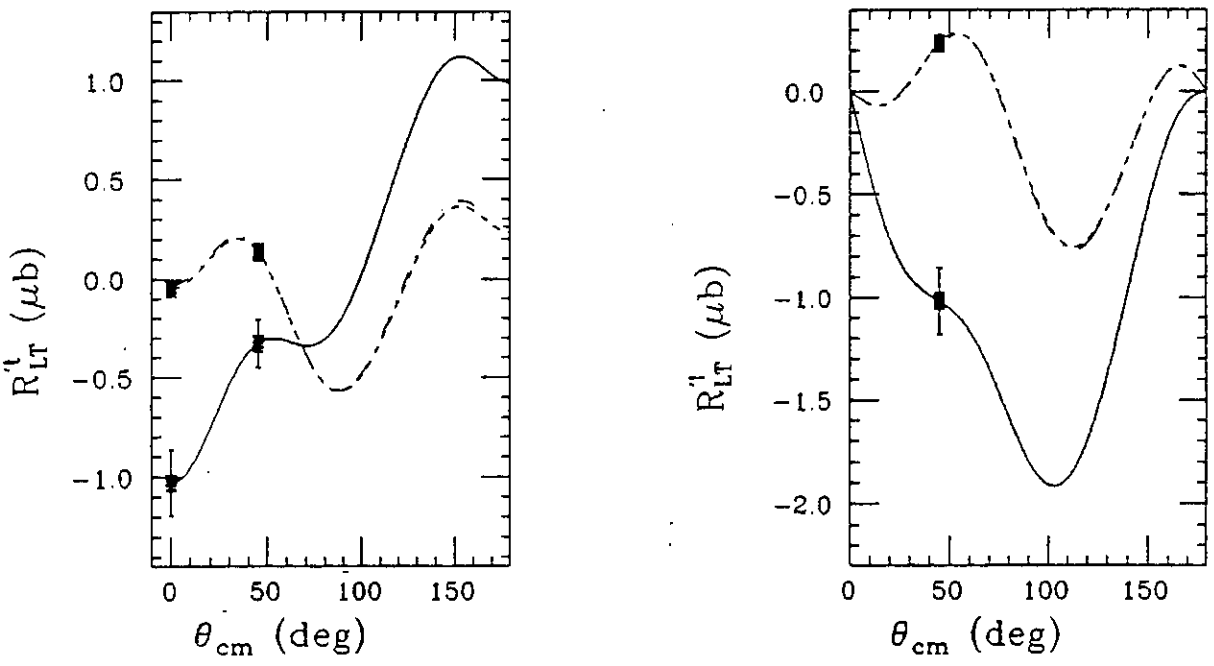

Figure 19. Response functions R'^t_{LT} and R'^ℓ_{LT} for pion electroproduction at W=1.440 GeV and Q^2=0.68 $(GeV/c)^2$. Solid curve: conventional quark radial excitation. Dot-dashed curve: hybrid state. The error bars are projected results of the proposed CEBAF experiment 91-011 (from ref. [54]).

Measurement of radiative decays of excited hyperon states - $\Sigma^*(1385)$, $\Delta^*(1405)$, $\Delta^*(1520)$ - yields information about the quark wave function of the hyperon. Clearly, an energy tagged photon beam and a $\sim 4\pi$ solid angle coverage for photon detection are needed for these experiments[59].

Electroproduction studies of the reactions $ep \rightarrow eK^*\Lambda$ and $ep \rightarrow eK^*\Lambda^*(1520)$, with measurement of the hyperon decay products, has been designed to learn about the reaction mechanism and the K^+ and $K^{*+}(892)$ form factors. At the same time, the electroproduction and decay of the $f_o(975)$ will be measured. This state, which does not fit in the normal $q\bar{q}$ scheme, could possibly be an exotic $qq\bar{q}\bar{q}$ state or a $q\bar{q}$ - $q\bar{q}$ molecule. Using the CLAS detector at $10^{34}cm^{-2}s^{-1}$ luminosity, one expects the number of detected events per hour to be 400, 1600 and 1100 for f_o, Λ and $\Lambda^*(1520)$ respectively[60].

VI. Conclusion

The CEBAF beams, with a unique combination of high energy, high duty factor, high intensity and high definition open new possibilities for the study of nucleons and nuclei at short distances. A broad physics program is planned, from elastic scattering to several GeV excitation energies. High Q^2 measurements will explore the limits of a "nucleons and mesons" description of nuclei and the role of quark and gluon degrees of freedom. Emphasis is put on coincidence and polarization experiments. Experimental equipments include high resolution magnetic spectrometers as well as low luminosity, nearly 4π detectors. User collaborations have been formed, which are taking major responsibilities in the design, construction and testing of these equipments. New collaborators would be very welcome! The first beam to an experiment is scheduled for 1994.

References

[1] R. Holt, 4th Conference on Intersections Between Particle and Nuclear Physics, Tucson, AZ, 24-29 May 1991.

[2] C. Marchand et al., Phys. Lett. **B153** (1985)29.

[3] H.A. Grunder, Proc. 4th Workshop on Perspectives in Nuclear Physics at Intermediate Energies, ICTP, Italy, May 8-12, 1989, S. Boffi, C. Ciofi degli Atti and M. Giannini eds., World Scientific, Singapore (1989).

[4] L.S. Cardman, et al., University of Illinois Technical Note TN-89-4 (1989).

[5] Conceptual Design Report - Basic Experimental Equipment, CEBAF (1990).

[6] D.G. Crabb et al., Phys. Rev. Lett **64**, 2627 (1990).

[7] R. Madey et al., IEEE Transactions on Nuclear Science **36**, 231 (1989).

[8] A. Zondervan et al., Topical Workshop on Two-Nucleon Emission Reactions, EIPC, Elba, Italy, 19-23 Sept. 1989.

[9] S. Frullani et al., "Multi Purpose Spetrometer", INFN-ISS 90/5 (1990).

[10] R. Arnold et al., Phys. Rev. Lett. **57**, 174 (1986).

[11] P. Bosted, 4th Conf. on Intersections on Particle and Nuclear Physics, Tucson, AZ, May 23-29, 1991. NPAS-TN-91-1 (1991).

[12] R.G. Arnold, C.E. Carlson and F. Gross, Phys. Rev. **23**, 363 (1981).

13] CEBAF proposal 89-014, C.F. Perdrisat and V. Punjabi spokespersons (9989).

[14] S. Platchkov et al., Nucl. Phys. **A510**, 740 (1990).

[15] CEBAF proposal 89-005, R. Madey spokesperson (1989).
[16] CEBAF proposal 89-108, D. Day spokesperson (1989).
[17] "SAMPLE Collaboration": D.M. Beck, E. Beise, E. Blez, L. Cardman, R. Carlini, R. Carr, G. Dodson, K. Dow, M. Farkhondeh, B. Filipone, S. Kowalski, W. Lorenzon, R. McKeown and J. Napolitano, MIT-Bates Experiment 89-06 (1989).
[18] J. Napolitano, Phys. Rev. **C43**, 1473 (1991).
[19] R.L. Jaffe, Phys. Lett. **B229**, 275 (1989).
[20] CEBAF proposal 91-010, J.M. Finn and P. Souder spokespersons (1991).
[21] CEBAF proposal 91-004, E. Beise spokesperson (1991).
[22] CEBAF proposal 91-017, D. Beck spokesperson (1991).
[23] S. Frullani and J. Mougey, Adv. Nucl. Phys. **14**, 1 (1984).
P.K.A. deWitt Huberts, J. Phys. G. **16**, 507 (1990).
[24] J.W.A. Den Herder et al., Nucl. Phys. **A490**, 507 (1988).
[25] G. van der Steenhoven et al., Nucl. Phys. **A480**, 547, (1988).
[26] P.E. Ulmer et al., Phys. Rev. Lett. **59**, 2259 (1987).
[27] G. van der Streenhoven et al., Phys. Rev. Lett. **57**, 182 (1986) and Phys. Rev. Lett. **58**, 1727 (1987).
[28] D Reffay-Pikeroen et al., Phys. Rev. Lett. **60**, 776 (1988).
[29] C. Marchand et al., Phys. Rev. Lett. **60**, 1703 (1988).
[30] R.W. Lourie et al., Phys. Rev. Lett. **56**, 2364 (1986).
[31] A. Pickelsimer and J.W. Van Orden, Phys. Rev. **C40**, 290 (1989).
[32] CEBAF proposal 89-025, J.M. Finn and P. Ulmer spokespersons (1989).
[33] CEBAF proposal 89-028, J.M. Finn and P. Ulmer spokespersons (1989).
[34] H. Arenhövel, W. Leidemann and E.L. Tomusiak, Z. Phys. **A331**, 123 (1988); erratum Z. Phys. **A334**, 363 (1989 and private communication (1989).
[35] A.Yu. Korchin, Yu.P. Melnik and A.V. Shebeko, Few Body Systems **9**, 211 (1990).
[36] M.P. Rekalo, G.I. Gakh and A.P. Rekalo, J. Phys. **G15**, 1223 (1989).
[37] F. Gross and J.W. Van Orden, private communication (1990).
[38] J.M. Legoff et al., 4th Workshop on Perspectives in Nuclear Physics at Intermediate Energies, S. Boffi et al., eds., World Scientific (1989), p. 376.
[39] CEBAF proposal 89-044, M. Epstein, R. Lourie and J. Mougey spokespersons (1989).
[40] CEBAF proposal 89-003, R. Lourie, W. Bertozzi, L. Weinstein and A. Saha spokespersons (1989).
[41] CEBAF proposal 89-027, W. Bertozzi, W. Boeglin, L. Weinstein spokespersons (1989).
CEBAF proposal 89-031, W. Hersman, J. Lightbody, R.A. Miskimen spokespersons (1989).
[42] CEBAF proposal 89-029, H.P. Blok spokesperson (1989).
[43] CEBAF proposal 89-030, R. A. Lindgren, M. Epstein, G. J. Lolos, Z.-E. Meziani spokespersons (1989).
[44] J.M. Laget, J. Phys. **G14**, 1445 (1988).
[45] A. Magnon et al., Phys. Lett. **B222**, 352 (1989); C. Marchand, G. Salmè and S. Simula, Nucl. Phys. **A532**, 301c (1991).
[46] K.F. von Reden et al., Phys. Rev. **C41**, 1084 (1990).
[47] Z.-E. Meziani et al.,submitted to Phys. Rev. Letters (1992).

[48] CEBAF proposal 91-007, R.G. Milner spokesperson (1991).
CEBAF proposal 91-013, D. Geesaman spokesperson (1991).
[49] CEBAF proposal 91-006, A. Saha spokesperson (1991).
[50] R. Koniuk and N. Isgur, Phys. Rev. **D21**, 1888 (1980).
F.E. Close and Zhenping Li, Phys. Rev. **D42**, 2194 (1990).
[51] V. Burkert, Nucl. Phys. B (Proc. Suppl.) **21**, 287 (1991).
[52] CEBAF proposal 89-037, V. Burkert, R. Minehart spokespersons (1989).
[53] CEBAF proposal 89-042, V. Burkert, R. Minehart spokespersons (1989).
[54] CEBAF proposal 91-011, S. Frullani and R. Lourie spokespersons (1991).
[55] Zhenping Li, V. Burkert and Zhujun Li, CEBAF preprint PR-91-032 (1991).
[56] H.J. Weber, in *Progress in Nuclear Physics*, W.-Y. P. Hwang et al., eds., Elsevier (1991), p. 206.
[57] CEBAF proposal 89-040, P. Stoler and V. Burkert spokespersons (1989).
[58] CEBAF proposal 89-004, R. Schumacher spokesperson (1989).
[59] CEBAF proposal 89-024, G.S. Mutchler spokesperson (1989).
[60] CEBAF proposal 89-043, L. Dennis and H. Funsten spokespersons (1989).